Hindawi
International Journal of Antennas and Propagation
Volume 2020, Article ID 9710723, 13 pages
https://doi.org/10.1155/2020/9710723

Research Article

Quasi-Static Solution for ELF/SLF near-Zone Field of a Vertical Magnetic Dipole near the Surface of a Lossy Half-Space

Lina He,[1] Tong He,[2] and Kai Li[1]

[1]*College of Information Science and Electronic Engineering, Zhejiang University, Hangzhou 310027, China*
[2]*Intelligent Network Research Center, Zhejiang Lab, Hangzhou 311100, China*

Correspondence should be addressed to Tong He; tongh@zhejianglab.com

Received 28 October 2019; Revised 29 January 2020; Accepted 4 February 2020; Published 20 March 2020

Academic Editor: Ana Alejos

Dipole antennas over the boundary between two different media have been widely used in the fields of geophysics exploration, oceanography, and submerged communication. In this paper, an analytical method is proposed to analyse the near-zone field at the extremely low frequency (ELF)/super low frequency (SLF) range due to a vertical magnetic dipole (VMD). For the lack of feasible analytical techniques to derive the components exactly, two reasonable assumptions are introduced depending on the quasi-static definition and the equivalent infinitesimal theory. Final expressions of the electromagnetic field components are in terms of exponential functions. By comparisons with direct numerical solutions and exact results in a special case, the correctness and effectiveness of the proposed quasi-static approximation are demonstrated. Simulations show that the smallest validity limit always occurs for component H_{2z}, and the value of $k_2\rho$ should be no greater than 0.6 in order to keep a good consistency.

1. Introduction

The propagation properties of extremely low frequency (ELF: 3–30 Hz) and super low frequency (SLF: 30–300 Hz) waves over the boundary between two different media have been extensively investigated for many years because of their useful applications in geophysics exploration, oceanography, overwater or underwater communication, and so on. For example, the US system Seafarer, operated at the frequency of 78 Hz [1], while the Russian one, called ZEVS, operated at the frequency of 82 Hz [2]. These systems have been used to communicate from a fixed station on the sea surface with a submarine traveling close to the ocean floor since 1990s [3, 4]. The original expression of this problem can date back to 1909 by Sommerfeld in his classic literature [5]. Subsequently, Norton proposed simple formulas and graphs in 1936 [6]. Following their works, many other progresses were made on numerical [7, 8] and analytical solutions [9–15] at a large propagation distance of $k\rho \gg 1$, where k represents the wave number and ρ is the propagation distance.

Evidently, in practical physical models such as a dipole source on the interface between two different media like air and Earth or sea water and rock, the electric propagation distance for the ELF/SLF ranges is usually very small, namely, $k\rho \ll 1$. Sommerfeld integrals are used for field components which can be expressed in terms of the derivatives of integrals including the Bessel function. Due to the divergence terms in Sommerfeld integrals, the investigation of ELF/SLF near-zone field is still not well developed yet. In the recent work by Xu et al. [16], a new quasi-static technique is used for analyzing the near-zone field radiated by a horizontal electric dipole near the sea-rock boundary. This new development rekindled our interest in investigating the magnetic-dipole excitation problem.

Several investigations of simplifying formulas had been made by Banos and Wesley [17]. They obtained approximation solutions suitable for both near and far fields in terms of Hertz potentials. Based on their efforts, Durrani [18, 19] addressed the sufficiently accurate but relatively simple field components in the sea produced by vertical and horizontal dipoles (both electric and magnetic types) under reasonable limitations. Also of interest is the satisfactory communication range between air and sea. Later on, in a series of papers by Bannister [20, 21], previous

theoretical work like [22] was well summarized, and all field components for these four different types of dipoles located on the boundary were presented over the quasi-static range. In recent years, some near-field research has gradually been carried out both analytically [23–25] and numerically [26]. Particularly in 2010, Parise [27] established the exact closed-form expressions of the electromagnetic field components excited by a vertical magnetic dipole lying on the surface of a flat and homogeneous lossy half-space, but unfortunately H_ρ is still in terms of Bessel functions, and these formulas are valid only when both of the dipole source and the observation point are embedded on the boundary. In many practical applications, both the dipole source and the receiving point may be located near the boundary. However, the corresponding study on this near-field radiation of a vertical magnetic dipole is still in the dark. Since it is a formidable task to calculate it accurately by existing analytical methods, in this paper, we will attempt to extend the work by Xu et al. [16] and evaluate the integrals in purpose of deriving new approximation formulas.

Note that the propagation distance of interest is up to dozens of kilometers, in this case, the propagation path via the reflection of the ionosphere is much longer than that along the Earth's surface. Hence, the effect of the ionosphere can be neglected and a simple half-space flat model is established. At ELF/SLF ranges, media such as sea water/ground/Earth are always regarded as highly lossy ones, while the air is lossless. So, the ratio of the wave numbers is far smaller than 1, i.e., $k_{air}/|k_{media}| \ll 1$. Furthermore, usually the heights of both the dipole source and the receiving point are much smaller than the horizontal distance, i.e., $d \ll \rho$ and $z \ll \rho$. The following are some concrete evaluations and simplifications. Comparisons with direct numerical simulations and exact solutions are also carried out from both the amplitude and phase angle aspects eventually. The time dependence $e^{i\omega t}$ is assumed and suppressed throughout the analysis.

2. Formulations

The geometry and notations of the physical model are shown in Figure 1. It consists of a loop antenna (viewed as a vertical magnetic dipole) situated at a distance d, above a half-infinite conducting space. Cartesian and cylindrical coordinates are introduced with z directed upwards through the dipole, and the radius ρ is taken horizontally in the x-y plane on the surface. The air characterized by the parameters ε_2, μ_2, and σ_2 occupies the upper space ($z \geq 0$), and the lossy medium (like seawater or Earth) characterized by the parameters ε_1, μ_1, and σ_1 occupies the lower space ($z \leq 0$). It is assumed that both regions are nonmagnetic so that $\mu_1 = \mu_2 = \mu_0$.

2.1. Integral Expressions for the Field Excited by an ELF/SLF VMD. When its size is small enough compared with the propagation distance and free-space wavelength, it is a fairly common-sense idea to regard a small current loop as a vertical magnetic dipole (VMD) [28]. We identify IdS as the magnetic dipole moment, where I denotes the loop circulating current and dS represents the area of the loop. With a similar method by King [29], the integrals for the components of the electromagnetic field in Region 2 can be written as follows:

$$E_{2\varphi}(\rho, z) = -\frac{\omega\mu_0 IdS}{2\pi}\int_0^\infty \left[\frac{e^{i\gamma_2|z-d|}}{2\gamma_2} - \frac{e^{i\gamma_2(z+d)}}{2\gamma_2} + \frac{e^{i\gamma_2(z+d)}}{\gamma_1+\gamma_2}\right] J_1(\lambda\rho)\lambda^2 \mathrm{d}\lambda, \tag{1}$$

$$H_{2\rho}(\rho, z) = \frac{IdS}{2\pi}\int_0^\infty \left[\pm\frac{e^{i\gamma_2|z-d|}}{2} - \frac{e^{i\gamma_2(z+d)}}{2} + \frac{\gamma_2 e^{i\gamma_2(z+d)}}{\gamma_1+\gamma_2}\right] J_1(\lambda\rho)\lambda^2 \mathrm{d}\lambda, \tag{2}$$

$$H_{2z}(\rho, z) = i\frac{IdS}{2\pi}\int_0^\infty \left[\frac{e^{i\gamma_2|z-d|}}{2\gamma_2} - \frac{e^{i\gamma_2(z+d)}}{2\gamma_2} + \frac{e^{i\gamma_2(z+d)}}{\gamma_1+\gamma_2}\right] J_0(\lambda\rho)\lambda^3 \mathrm{d}\lambda. \tag{3}$$

where

$$\gamma_n = \sqrt{k_n^2 - \lambda^2}, \quad n = 1, 2. \tag{4}$$

It is noted that the upper sign "+" in (2) corresponds to $z > d$, and the lower sign "–" corresponds to $0 < z < d$, respectively. And the square root in (4) is taken in the first quadrant.

The first two terms in formulas (1)–(3) stand for the direct wave and the ideal reflected wave. Meanwhile, the third term represents the lateral wave. Thus, these formulas can be rewritten in the following forms:

$$\begin{aligned} E_{2\varphi}(\rho, z) &= E_{2\varphi}^d(\rho, z) + E_{2\varphi}^i(\rho, z) + E_{2\varphi}^l(\rho, z), \\ H_{2\rho}(\rho, z) &= H_{2\rho}^d(\rho, z) + H_{2\rho}^i(\rho, z) + H_{2\rho}^l(\rho, z), \\ H_{2z}(\rho, z) &= H_{2z}^d(\rho, z) + H_{2z}^i(\rho, z) + H_{2z}^l(\rho, z). \end{aligned} \tag{5}$$

In the above integrals, the direct-field and reflect-field terms can be derived via the method presented in the monograph by King et al. [15].

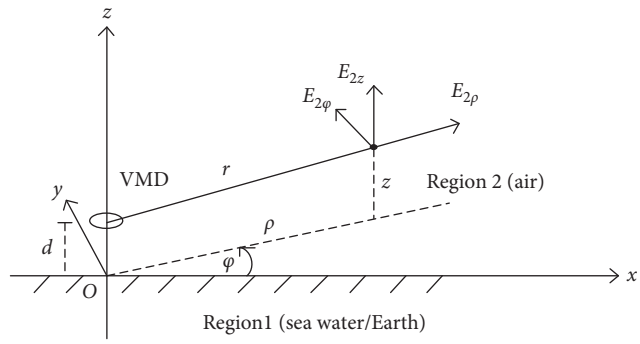

Figure 1: Excitation of an ELF/SLF VMD above a lossy half-space.

The direct-field components are

$$
\begin{aligned}
E_{2\varphi}^{d}(\rho,z) &= -\frac{\omega\mu_0 IdS}{4\pi}\int_0^{\infty}\frac{e^{i\gamma_2|z-d|}}{\gamma_2}J_1(\lambda\rho)\lambda^2\mathrm{d}\lambda = \frac{\omega\mu_0 IdS}{4\pi}\rho k_2\left(\frac{1}{r_1^2}+\frac{i}{k_2 r_1^3}\right)e^{ik_2 r_1},\\
H_{2\rho}^{d}(\rho,z) &= \pm\frac{IdS}{4\pi}\int_0^{\infty}e^{i\gamma_2|z-d|}J_1(\lambda\rho)\lambda^2\mathrm{d}\lambda = \mp\frac{IdS}{4\pi}\rho k_2\left(\frac{d_1}{r_1}\right)\left(\frac{k_2}{r_1^2}+\frac{3i}{r_1^3}-\frac{3}{k_2 r_1^4}\right)e^{ik_2 r_1},\\
H_{2z}^{d}(\rho,z) &= i\frac{IdS}{4\pi}\int_0^{\infty}\frac{e^{i\gamma_2|z-d|}}{\gamma_2}J_0(\lambda\rho)\lambda^3\mathrm{d}\lambda = -i\frac{IdS}{4\pi}\left[k_2\left(\frac{ik_2}{r_1}-\frac{1}{r_1^2}-\frac{i}{k_2 r_1^3}\right)e^{ik_2 r_1}+\frac{k_2 d_1^2}{r_1^2}\left(\frac{ik_2}{r_1}-\frac{3}{r_1^2}-\frac{3i}{k_2 r_1^3}\right)e^{ik_2 r_1}\right].
\end{aligned}
\tag{6}
$$

The reflect-field components are

$$
\begin{aligned}
E_{2\varphi}^{i}(\rho,z) &= -\frac{\omega\mu_0 IdS}{4\pi}\int_0^{\infty}\frac{e^{i\gamma_2(z+d)}}{\gamma_2}J_1(\lambda\rho)\lambda^2\mathrm{d}\lambda = \frac{\omega\mu_0 IdS}{4\pi}\rho k_2\left(\frac{1}{r_2^2}+\frac{i}{k_2 r_2^3}\right)e^{ik_2 r_2},\\
H_{2\rho}^{i}(\rho,z) &= \frac{IdS}{4\pi}\int_0^{\infty}e^{i\gamma_2(z+d)}J_1(\lambda\rho)\lambda^2\mathrm{d}\lambda = -\frac{IdS}{4\pi}\rho k_2\left(\frac{d_2}{r_2}\right)\left(\frac{k_2}{r_2^2}+\frac{3i}{r_2^3}-\frac{3}{k_2 r_2^4}\right)e^{ik_2 r_2},\\
H_{2z}^{i}(\rho,z) &= i\frac{IdS}{4\pi}\int_0^{\infty}\frac{e^{i\gamma_2(z+d)}}{\gamma_2}J_0(\lambda\rho)\lambda^3\mathrm{d}\lambda\\
&= -i\frac{IdS}{4\pi}\left[k_2\left(\frac{ik_2}{r_2}-\frac{1}{r_2^2}-\frac{i}{k_2 r_2^3}\right)e^{ik_2 r_2}+\frac{k_2 d_2^2}{r_2^2}\left(\frac{ik_2}{r_2}-\frac{3}{r_2^2}-\frac{3i}{k_2 r_2^3}\right)e^{ik_2 r_2}\right].
\end{aligned}
\tag{7}
$$

where

$$
\begin{aligned}
d_1 &= |z-d|,\\
d_2 &= z+d,\\
r_1 &= \sqrt{\rho^2+d_1^2},\\
r_2 &= \sqrt{\rho^2+d_2^2}.
\end{aligned}
\tag{8}
$$

The rest lateral-wave terms are defined by

$$
\begin{aligned}
E_{2\varphi}^{l}(\rho,z) &= -\frac{\omega\mu_0 IdS}{2\pi}\int_0^{\infty}\frac{1}{M}e^{i\gamma_2(z+d)}J_1(\lambda\rho)\lambda^2\mathrm{d}\lambda\\
&= -\frac{\omega\mu_0 IdS}{2\pi}\cdot F_{2\varphi}^{l}(\rho,d_2),
\end{aligned}
\tag{9}
$$

$$
\begin{aligned}
H_{2\rho}^{l}(\rho,z) &= \frac{IdS}{2\pi}\int_0^{\infty}\frac{\gamma_2}{M}e^{i\gamma_2(z+d)}J_1(\lambda\rho)\lambda^2\mathrm{d}\lambda\\
&= \frac{IdS}{2\pi}\cdot F_{2\rho}^{l}(\rho,d_2),
\end{aligned}
\tag{10}
$$

$$H_{2z}^{l}(\rho,z) = i\frac{IdS}{2\pi}\int_0^\infty \frac{1}{M}e^{i\gamma_2(z+d)}J_0(\lambda\rho)\lambda^3\mathrm{d}\lambda = i\frac{IdS}{2\pi}\cdot F_{2z}^{l}(\rho,d_2), \tag{11}$$

where $M = \gamma_1 + \gamma_2$. It should be pointed out that these formulas contain Bessel functions, whose integrands are highly oscillatory in the near-zone. Therefore, a novel approximation approach is required to be taken into consideration in the following subsection.

2.2. Simplifications of the Lateral-Wave Terms under the Equivalent Infinitesimal Theory. For the beginning of simplification, we should figure out the definition of "quasi-static" or "near-field" involved in this paper. It is defined as the situation where the distance from the source to the observation point is far less than a wavelength ($k\rho \ll 1$) [15, 18]. Typically, if the frequency remains invariable, distances satisfying this condition contain the "near-field"; otherwise, if the distance is fixed, qualified frequencies form the "quasi-static" state.

It is readily understood from the definition, when the "quasi-static" assumption is considered, $\omega \longrightarrow 0$ and $k_2\rho \ll 1$ hold. Under this circumstance, contribution of the Sommerfeld integrals in (9)–(11) is mainly from the integration path where $\lambda \gg k_2$. Therefore, the parameter γ_2 can be expressed as follows:

$$\gamma_2 = \sqrt{k_2^2 - \lambda^2} \approx i\lambda. \tag{12}$$

Normally, the medium in Region 1 is highly conductive when compared with air in Region 2, namely, $k_2 \ll k_1$. Also, d and z are usually far less than the horizontal distance ρ, i.e., $d \ll \rho$ and $z \ll \rho$. Thus, we have

$$i\left|\gamma_1 - \gamma_2 - k_1\right|d_m \approx i\left|\sqrt{k_1^2 - \lambda^2} - i\lambda - k_1\right|d_m \ll 1, \tag{13}$$

where $m = 1, 2$. It is seen from (13) that the limit of $i|\gamma_1 - \gamma_2 - k_1|d_m$ can be approximated as zero. The equivalent infinitesimal theory, a special case of Taylor's formula, could be subsequently applied here as follows:

$$e^{i(\gamma_1-\gamma_2-k_1)d_m} - 1 \approx i(\gamma_1 - \gamma_2 - k_1)d_m. \tag{14}$$

Then, by some deformation, a useful alternative form of $\gamma_1 - \gamma_2$ is correspondingly obtained, so is the variable M. We write

$$\gamma_1 - \gamma_2 = i\frac{1 - e^{i(\gamma_1-\gamma_2-k_1)d_m}}{d_m} + k_1, \tag{15}$$

$$\frac{1}{M} = \frac{1}{\gamma_1+\gamma_2} = \frac{\gamma_1-\gamma_2}{(\gamma_1+\gamma_2)(\gamma_1-\gamma_2)} = i\frac{-e^{i(\gamma_1-\gamma_2-k_1)d_m} + 1 - ik_1d_m}{(k_1^2-k_2^2)d_m}. \tag{16}$$

Hence, by substituting (16) into (9), we have

$$F_{2\varphi}^{l}(\rho,d_2) = \int_0^\infty i\frac{-e^{i(\gamma_1-\gamma_2-k_1)(z+d)} + 1 - ik_1(z+d)}{(k_1^2-k_2^2)(z+d)}e^{i\gamma_2(z+d)}J_1(\lambda\rho)\lambda^2\mathrm{d}\lambda = \frac{-i}{(k_1^2-k_2^2)d_2}\left[e^{-ik_1d_2}\int_0^\infty e^{i(\gamma_1-k_1)d_2}J_1(\lambda\rho)\lambda^2\mathrm{d}\lambda + (ik_1d_2-1)\int_0^\infty e^{i\gamma_2d_2}J_1(\lambda\rho)\lambda^2\mathrm{d}\lambda\right]. \tag{17}$$

Similarly, (10) is equal to

$$F_{2z}^{l}(\rho,d_2) = \frac{-i}{(k_1^2-k_2^2)d_2}\left[e^{-ik_1d_2}\int_0^\infty e^{i(\gamma_1-k_1)d_2}J_0(\lambda\rho)\lambda^3\mathrm{d}\lambda + (ik_1d_2-1)\int_0^\infty e^{i\gamma_2d_2}J_0(\lambda\rho)\lambda^3\mathrm{d}\lambda\right]. \tag{18}$$

with $\int_0^\infty \gamma_2 e^{i\gamma_2 x}\mathrm{J}_1(\lambda P)\lambda^2 d\lambda = -i\partial/\partial x\int_0^\infty e^{i\gamma_2 x}\mathrm{J}_1(\lambda\rho)\lambda^2 d\lambda$, the remaining term $F_{2\rho}^{l}(\rho,d_2)$ in (10) can be evaluated as follows:

$$F_{2\rho}^{l}(\rho,d_2) = \int_0^\infty \frac{\gamma_2}{M}e^{i\gamma_2 z+d}\mathrm{J}_1(\lambda P)\lambda^2 d\lambda \approx \frac{\partial}{\partial d_2}\int_0^\infty\left[\frac{-e^{i(\gamma_1-\gamma_2-k_1)(z+d)} + 1 - ik_1(z+d)}{(k_1^2-k_2^2)(z+d)}\right]e^{i\gamma_2(z+d)}\mathrm{J}_1(\lambda\rho)\lambda^2\mathrm{d}\lambda = \frac{1}{k_1^2-k_2^2}\frac{\partial}{\partial d_2}\int_0^\infty\frac{-e^{i(\gamma_1-k_1)d_2} + (1-ik_1d_2)e^{i\gamma_2d_2}}{d_2}\mathrm{J}_1(\lambda\rho)\lambda^2\mathrm{d}\lambda. \tag{19}$$

Finally, with the Appendix in [15], the final analytical results for $F_{2\varphi}^{l}$, $F_{2\rho}^{l}$, F_{2z}^{l} can be obtained readily. We write

$$F_{2\varphi}^{l}(\rho,d_2)\approx\frac{\rho k_1}{r_2\left(k_1^2-k_2^2\right)}\left(\frac{k_1}{r_2^2}+\frac{3i}{r_2^3}-\frac{3}{k_1r_2^4}\right)e^{ik_1\left(r_2-d_2\right)}+\frac{\rho k_2\left(ik_1d_2-1\right)}{r_2\left(k_1^2-k_2^2\right)}\left(\frac{k_2}{r_2^2}+\frac{3i}{r_2^3}-\frac{3}{k_2r_2^4}\right)e^{ik_2r_2}, \tag{20}$$

$$\begin{aligned}F_{2\rho}^{l}(\rho,d_2)=&-\frac{i\rho}{\left(k_1^2-k_2^2\right)}\times\left[\frac{k_1^2}{r_2}\left(\frac{k_1}{r_2^2}+\frac{3i}{r_2^3}-\frac{3}{k_1r_2^4}\right)e^{ik_1\left(r_2-d_2\right)}-\frac{k_1d_2}{r_2^2}\left(\frac{k_1^2}{r_2^2}+\frac{6ik_1}{r_2^3}-\frac{15}{r_2^4}-\frac{15i}{k_1r_2^5}\right)e^{ik_1\left(r_2-d_2\right)}\right.\\&-k_1k_2\left(\frac{k_2}{r_2^3}+\frac{3i}{r_2^4}-\frac{3}{k_2r_2^5}\right)e^{ik_2r_2}+\frac{k_2d_2}{r_2^2}\left(\frac{k_2^2}{r_2^2}+\frac{6ik_2}{r_2^3}-\frac{15}{r_2^4}-\frac{15i}{k_2r_2^5}\right)e^{ik_2r_2}\\&\left.-k_1k_2\frac{d_2^2}{r_2^2}\left(\frac{ik_2^2}{r_2^2}-\frac{6k_2}{r_2^3}-\frac{15i}{r_2^4}+\frac{15}{k_2r_2^5}\right)e^{ik_2r_2}\right],\end{aligned} \tag{21}$$

$$F_{2z}^{l}(\rho,d_2)\approx\frac{k_1}{k_2^2-k_1^2}\left(\frac{k_1^2}{r_2^2}+\frac{4ik_1}{r_2^3}-\frac{9}{r_2^4}-\frac{9i}{k_1r_2^5}\right)e^{ik_1\left(r_2-d_2\right)}+\frac{k_2\left(ik_1d_2-1\right)}{k_2^2-k_1^2}\times\left(\frac{k_2^2}{r_2^2}+\frac{4ik_2}{r_2^3}-\frac{9}{r_2^4}-\frac{9i}{k_2r_2^5}\right)e^{ik_2r_2}. \tag{22}$$

So far, we have provided the process of calculating the field components for a VMD source over the near-field range in Region 2 in detail. The complete approximation solutions for the field components in Region 1 can be evaluated with a similar method as well.

2.3. Solutions for the near-Zone Field with $z = 0$ and $d = 0$. The complete quasi-static field components are derived readily with (9)–(11) and (20)–(22). For comparison purpose, in the following, we will attempt to reduce these formulas to the special case when both the dipole source and the receiving point are embedded on the boundary. For brevity and clarity, only H_{2z}'s derivation procedure is given as a demonstration. The magnetic component H_{2z} can be expressed as

$$\begin{aligned}H_{2z}=&\frac{IdS}{4\pi}k_2\left\{\left(\frac{k_2}{r_1}+\frac{i}{r_1^2}-\frac{1}{k_2r_1^3}\right)e^{ik_2r_1}-\frac{d_1^2}{r_1^2}\left(\frac{k_2}{r_1}+\frac{3i}{r_1^2}-\frac{3}{k_2r_1^3}\right)e^{ik_2r_1}\right.\\&-\left[\frac{k_2}{r_2}+\frac{i}{r_2^2}-\frac{1}{k_2r_2^3}-\frac{d_2^2}{r_2^2}\left(\frac{k_2}{r_2}+\frac{3i}{r_2^2}-\frac{3}{k_2r_2^3}\right)e^{ik_2r_2}+\frac{2ik_1}{k_2\left(k_1^2-k_2^2\right)}\left(\frac{k_1^2}{r_2^2}+\frac{4ik_1}{r_2^3}-\frac{9}{r_2^4}-\frac{9i}{k_1r_2^5}\right)e^{ik_1\left(r_2-d_2\right)}\right.\\&\left.\left.+\frac{2i-2k_1d_2}{k_1^2-k_2^2}\left(\frac{k_2^2}{r_2^2}+\frac{4ik_2}{r_2^3}-\frac{9}{r_2^4}-\frac{9i}{k_2r_2^5}\right)e^{ik_2r_2}\right].\right.\end{aligned} \tag{23}$$

Since $k_2\rho\ll1$ is assumed, with Maclaurin series, we have

$$e^{ik_2\rho}\approx1+ik_2\rho-\frac{\left(k_2\rho\right)^2}{2}. \tag{24}$$

By substituting (24) into (23) and setting $z = 0$, $d = 0$, it converts to:

$$H_{2z}\approx\frac{1}{2\pi}\left[\left(\frac{ik_1}{\rho^2}-\frac{4}{\rho^3}-\frac{9i}{k_1\rho^4}-\frac{9}{k_1^2\rho^5}\right)e^{ik_1\rho}+\frac{k_2^2}{k_1^2}\left(\frac{1}{\rho^3}+\frac{9}{\rho^5}\right)\right]. \tag{25}$$

Now, we have derived the analytical expressions when $z = d = 0$. To understand this method better, computations and discussions under several different conditions will be carried out in the following section.

3. Computation and Discussion

3.1. Comparison with Numerical Solutions When $z \neq 0$ and $d \neq 0$. It is shown in literature studies [7, 8] that, by some proper numerical approaches, one can solve Sommerfeld integrals directly. Therefore, direct numerical simulation is

employed and then compared with the analytical result obtained in this paper. We assume that Region 1 is seawater characterized by the permeability μ_0, relative permittivity $\varepsilon_{r1} = 80$, and conductivity $\sigma_1 = 4$ S/m. Region 2 is air characterized by the permeability μ_0 and the permittivity ε_0. For a general case, the dipole source and receiving point are placed at the height $d = 1$ m and $z = 5$ m, respectively. The amplitudes and phase angles of the three nonzero field components with respect to the propagation distance ρ are evaluated in Figures 2–4 at operating frequencies $f = 3$ Hz and 300 Hz.

It is seen that both the amplitudes and phase angles obtained by analytical and direct numerical methods have a consistent trend in general. Figures 2(a) and 2(b) show that at the beginning there exists a relatively apparent difference between these two computed results. This is probably because when ρ is too small, $d \ll \rho$ and $z \ll \rho$ are not very restrictive. But when $\rho > 10$ m, two curves shed light on a good correspondence with each other. The magnitude of $E_{2\varphi}$ and $H_{2\rho}$ in Figures 3(a), 3(b), 4(a), and 4(b) also show similar trends with H_{2z}. Obviously, in most cases of practical interest, $\rho \gg z$ and $\rho \gg d$, so the results confirm the high reliability and validity of the proposed method. Furthermore, it is also noted that the operating frequency has little influence to the magnitude of H_{2z} and $H_{2\rho}$, but a larger frequency will lead to a smaller amplitude of $E_{2\varphi}$.

As illustrated in Figures 2(c) and 2(d), initially the phase of H_{2z} ascend sharply until reaching the value of π. It is noted that a higher frequency leads to a closer mutation point to the source. Eventually, for a sudden change to $-\pi$, as the distance further increases, the phase starts rising smoothly and stabilizes around $-(\pi/2)$. Higher frequency also causes a faster phase variation from $-\pi$ to $-(\pi/2)$, which results in a shorter distance for reaching the final state. We can see that phase angles of the two methods are almost alike except with some latency. By observing other two components, though trajectories are not in full accord, similar conclusions can still be drawn.

It should also be born in mind that with large distances, $k_2\rho$ is more close to "1," which then also leads to a larger difference between the numerical and analytical results. In this paper, attention is restricted to the near field, and $k_2\rho \sim 1$ is out of consideration. Computations show that different components have different validity limits of $k_2\rho$ for maintaining a consistency between the proposal and numerical solutions. For $E_{2\varphi}$ and $H_{2\rho}$ components, results of both the amplitude and phase obtained by the two methods remain the same even if $k_2\rho$ is approaching 1. However, for H_{2z}, when the distance reaches 100 km (i.e., $k_2\rho \approx 0.6$, as can be seen in Figure 2(b)), two curves start to deviate from each other.

3.2. Comparison with Exact Solutions When $z = 0$ and $d = 0$. When both the dipole source and receiving point are located at the interface of a half-space, the exact field components excited by a vertical magnetic dipole have been addressed by Parise already [27]. The exact solutions of H_{2z}, $E_{2\varphi}$, and $H_{2\rho}$ can be expressed in terms of

$$
\begin{aligned}
(\text{exact})_z^{(\text{exact})} &= -\frac{IdS}{2\pi\left(k_2^2 - k_1^2\right)}\left(\widehat{Q}_2(\rho) - \widehat{Q}_1(\rho)\right),\\
(\text{exact})_\varphi^{(\text{exact})} &= -i\frac{IdS}{2\pi\left(k_2^2 - k_1^2\right)}\left(Q_2'(\rho) - Q_1'(\rho)\right),\\
(\text{exact})_\rho^{(\text{exact})} &= \frac{IdS}{\pi\rho}\left[\frac{\alpha^2 + \beta^2}{2}K_1(\alpha\rho)I_1(\beta\rho) - \alpha\beta K_2(\alpha\rho)I_2(\beta\rho)\right],
\end{aligned}
\tag{26}
$$

where

$$
\begin{aligned}
\widehat{Q}_n(\rho) &= \left(ik_n^3\rho^3 - 4k_n^2\rho^2 - 9ik_n\rho + 9\right)\frac{e^{ik_n\rho}}{\rho^5},\\
Q_n'(\rho) &= \left(k_n^2\rho^2 + 3ik_n\rho - 3\right)\frac{e^{ik_n\rho}}{\rho^4}.
\end{aligned}
\tag{27}
$$

Note that I_n and K_n are the nth order modified Bessel functions of the first and second kind, respectively, where $n = 1, 2$.

Since it is a special case of the dipole radiation problem discussed in this paper, we can actually better validate the manner if we plot how that field changes as a function of the distance ρ by our approximation method, the direct numerical calculation and this exact analytical solution. Comparisons are depicted in Figures 5–7. All the parameters involved are the same with those in Figures 2–4 except with different d and z.

Apparently, our analytical results not only coincide with the numerical simulations but also have an excellent agreement with the exact solutions, and curves in Figures 5–6 bear a strong resemblance to those in Figures 2–3. It indicates that all methods are of good accuracy. Meanwhile, comparisons of $H_{2\rho}$ are not satisfactory as can be seen from Figure 7. On the whole, curves of the analytical and numerical solution are relatively consistent, but do not match up to the exact solution as the propagation distance ρ increases. Take $f = 3$ Hz as an example. If ρ reaches several hundred meters, the gap in magnitude between exact solutions and the other two methods will become larger. And the phase difference is always about π. This is probably because the exact solution in [27] is expressed in terms of the modified Bessel functions rather than concrete analytical ones.

3.3. Evaluations for These Analytical Formulas. For further investigation about the features of the proposed method, several other evaluations are performed. As a natural extension, just to make it clear and to see how the locations of the dipole source and receiving point influence the propagation strength of electromagnetic fields, we consider the following simulations presented in Figure 8, with the relative permittivity $\varepsilon_{r1} = 80$ and conductivity $\sigma_1 = 4$ S/m in Region 1. The operating frequency is taken as $f = 10$ Hz.

Figure 8 illustrates the relationship between $|H_{2z}|$ and z with different heights of the source at a constant propagating distance, where all other parameters are held unchanged. The constant is chosen as 50 m, 100 m, 500 m, and 1000 m,

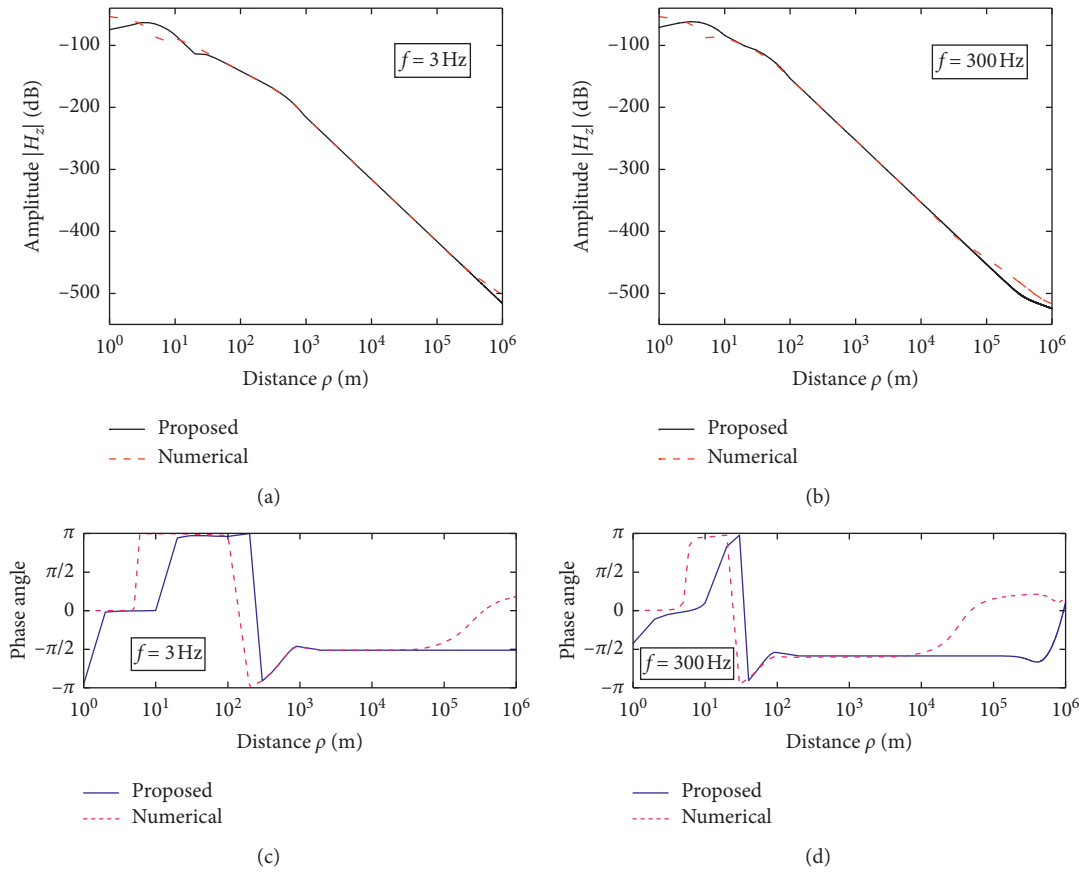

FIGURE 2: Amplitudes and phase angles of field component H_{2z} versus the propagation distance ρ with the proposed and numerical solutions. (a, c) $f = 3$ Hz. (b, d) $f = 300$ Hz.

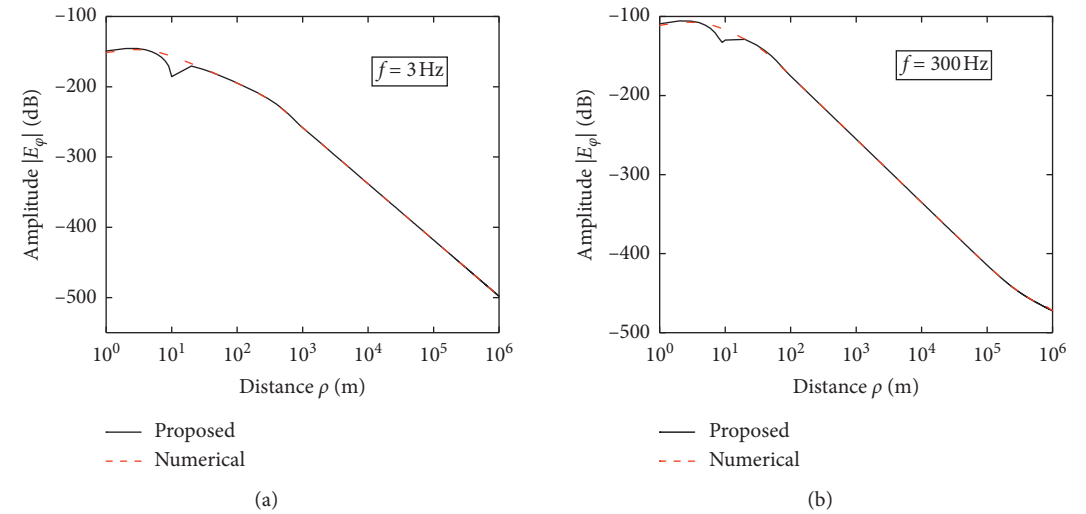

FIGURE 3: Continued.

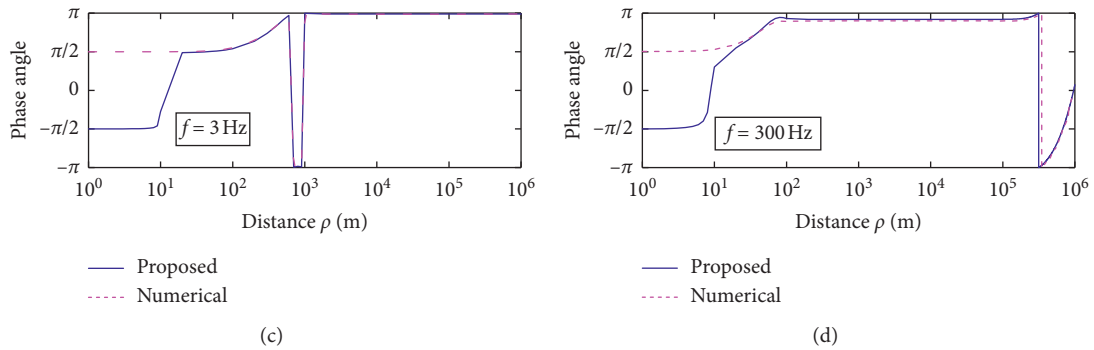

FIGURE 3: Amplitudes and phase angles of the field component $E_{2\varphi}$ versus the propagation distance ρ with the proposed and numerical solutions. (a, c) $f = 3$ Hz. (b, d) $f = 300$ Hz.

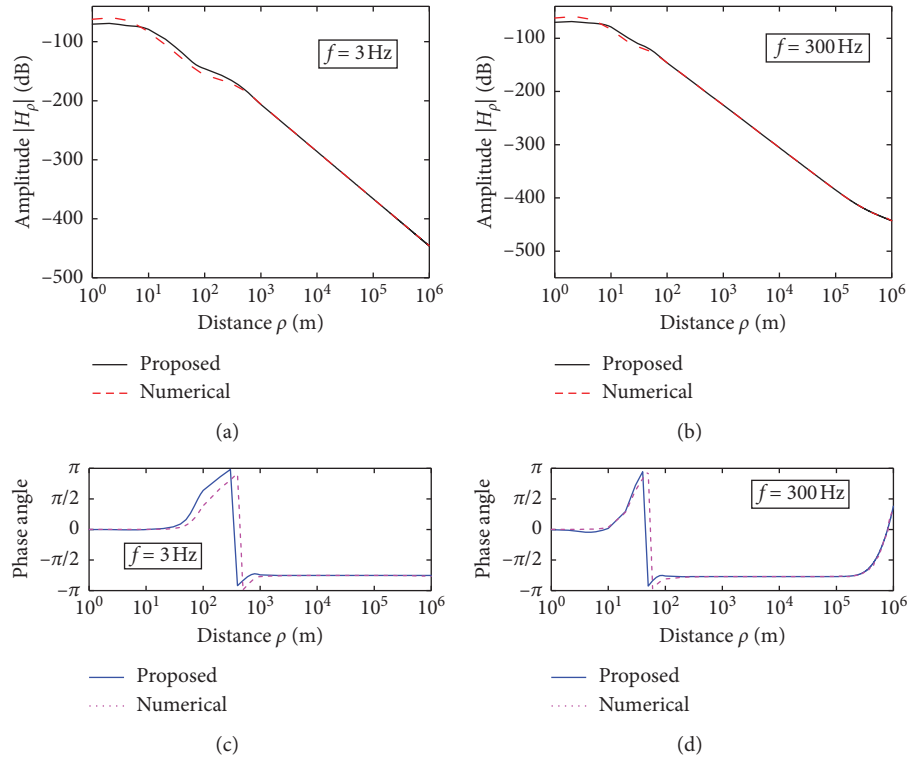

FIGURE 4: Amplitudes and phase angles of the field component $H_{2\rho}$ versus the propagation distance ρ with the proposed and numerical solutions. (a, c) $f = 3$ Hz. (b, d) $f = 300$ Hz.

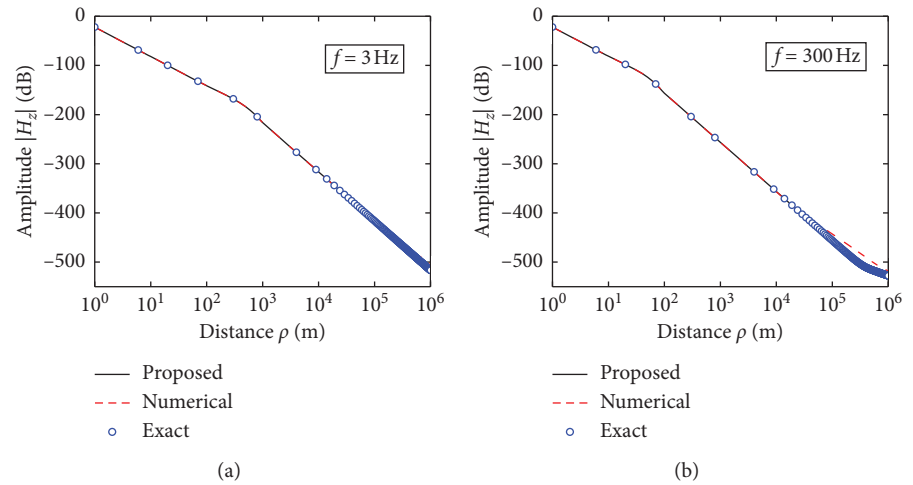

FIGURE 5: Continued.

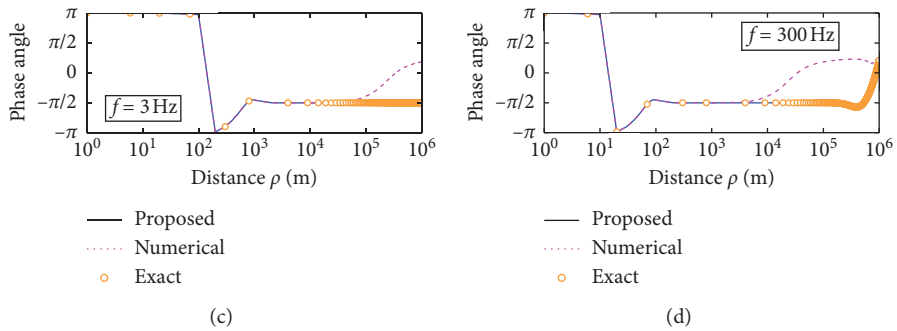

FIGURE 5: Amplitudes and phase angles of field component H_{2z} versus the propagation distance ρ with the proposed, exact, and numerical solutions. (a, c) $f = 3$ Hz. (b, d) $f = 300$ Hz.

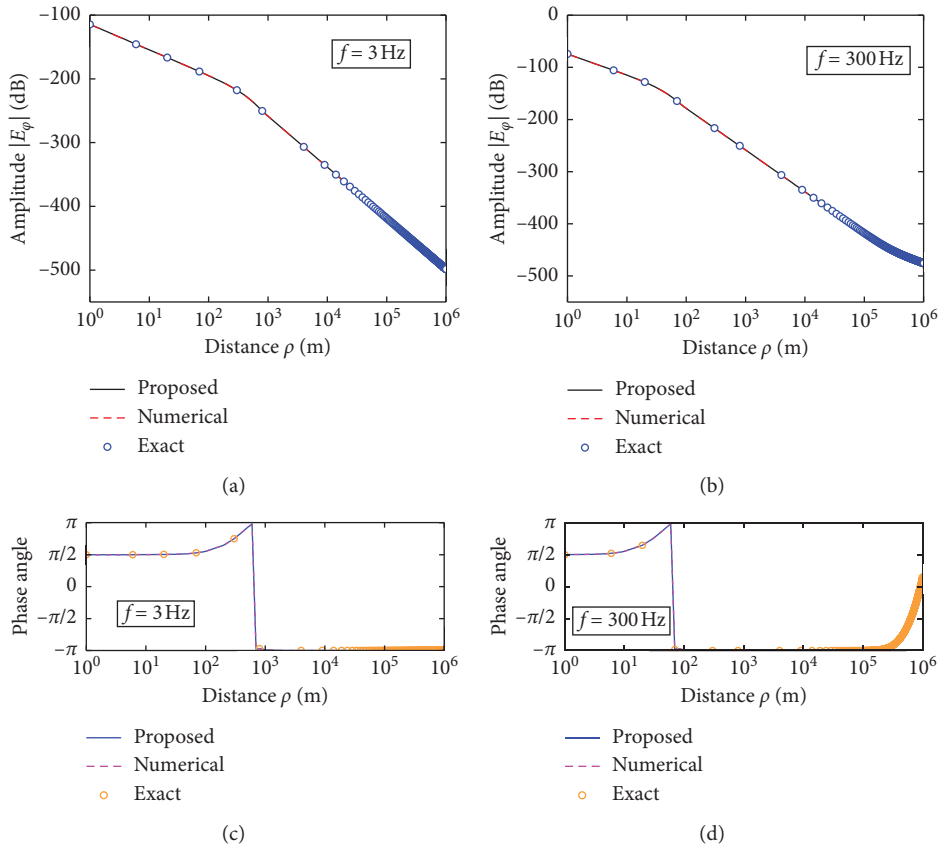

FIGURE 6: Amplitudes and phase angles of field component $E_{2\varphi}$ versus the propagation distance ρ with the proposed, exact, and numerical solutions. (a, c) $f = 3$ Hz. (b, d) $f = 300$ Hz.

respectively. It is seen that, with the increasing of the radial distance, $|H_{2z}|$ will exhibit quite different characteristics. When ρ is relatively small (see Figures 8(a) and 8(b)), the amplitude decreases at first and then increases gradually as the height of the observing point becomes higher. Typically, the minimum point of the curve will have a shift to a farther position from the origin if ρ is larger. However, for sufficiently large values of ρ (Figures 8(c) and 8(d)), the amplitude increases monotonically as z increases. We also know that, when the dipole source is closer to the interface, the attenuation will be larger. Perhaps it is due to the different degrees of the effect by the lossy medium in Region 1 at different heights.

When the receiving point is at an arbitrary place on the x-z plane in Region 2, and the dipole source is located at $d = 0$ m, 50 m, 150 m, respectively, with the operating frequency taken as $f = 10$ Hz, the strength distributions of the electric and magnetic components are revealed in Figures 9–10. We can actually see that both the electric and magnetic fields decay rapidly in all directions. As the position of the source is higher, the attenuation of the electromagnetic components will become slower. It is also noted that the distribution in

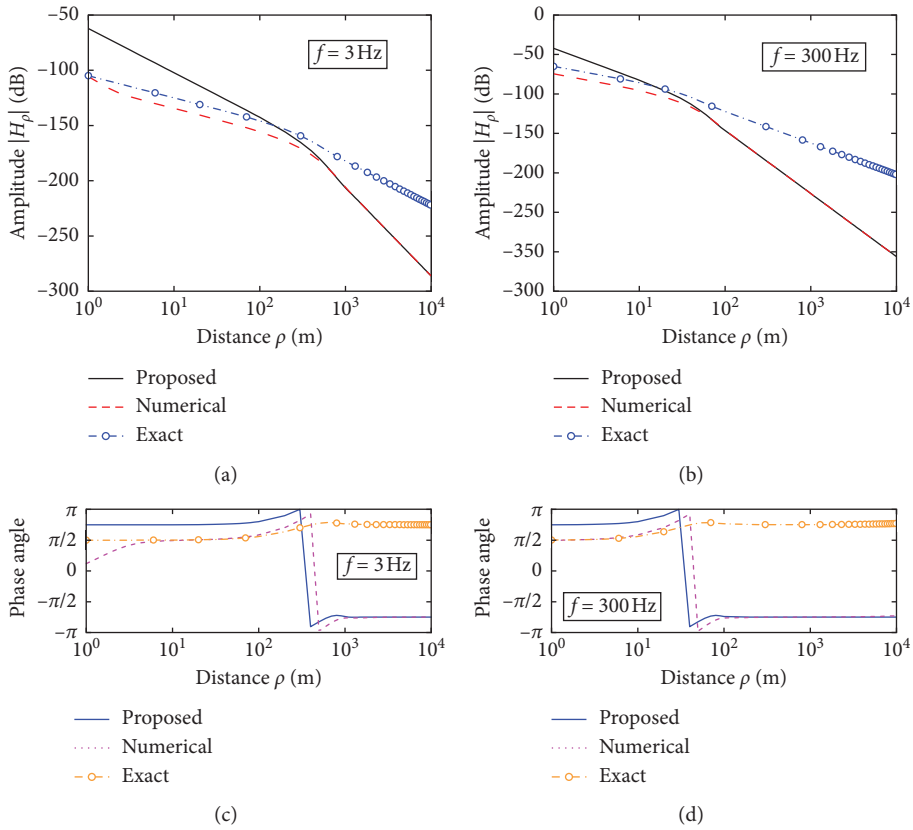

FIGURE 7: Amplitudes and phase angles of field component $H_{2\rho}$ versus the propagation distance ρ with the proposed, exact, and numerical solutions. (a, c) $f = 3$ Hz. (b, d) $f = 300$ Hz.

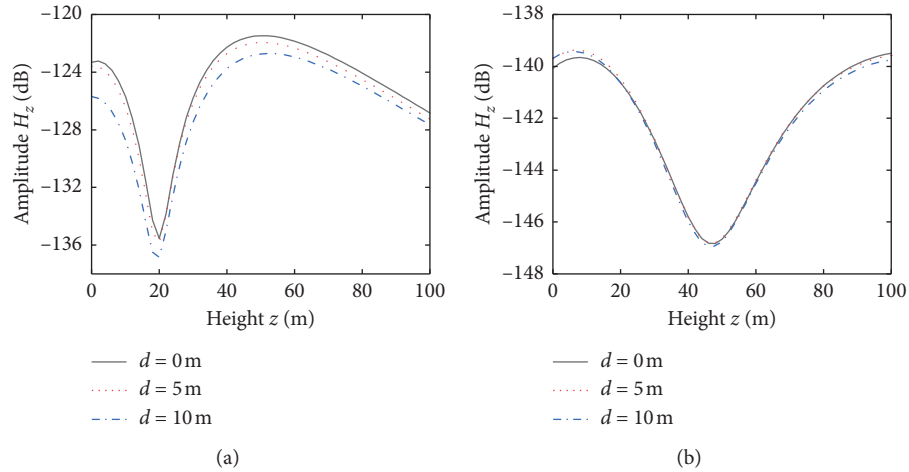

FIGURE 8: Continued.

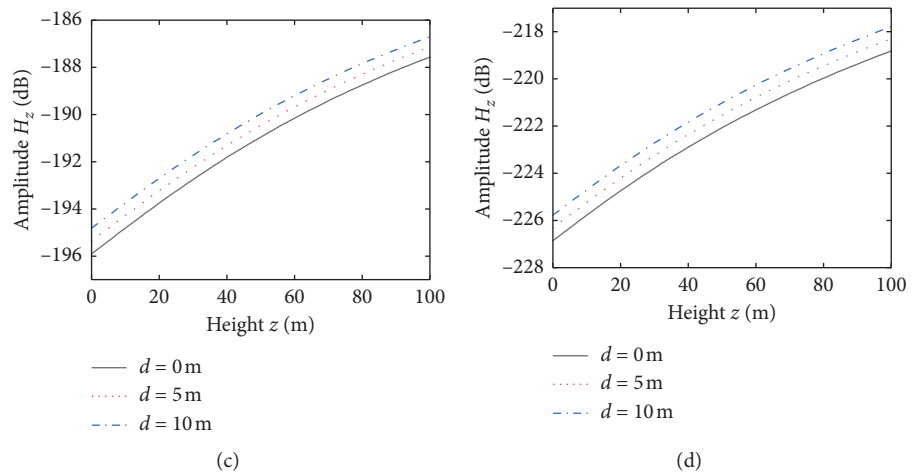

FIGURE 8: Amplitude of field component H_{2z} versus the receiving height z: (a) $\rho = 50$ m, (b) $\rho = 100$ m, (c) $\rho = 500$ m, and (d) $\rho = 1000$ m.

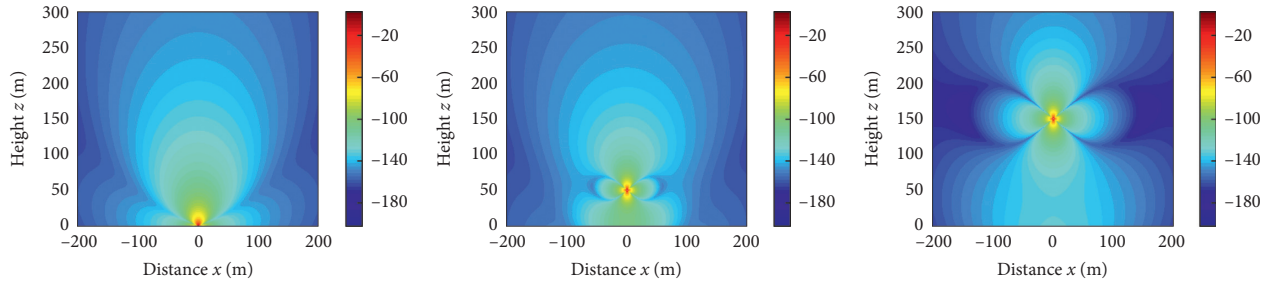

FIGURE 9: Field distribution of H_{2z} in the x-z plane: (a) $d = 0$ m, (b) $d = 50$ m, and (c) $d = 150$ m.

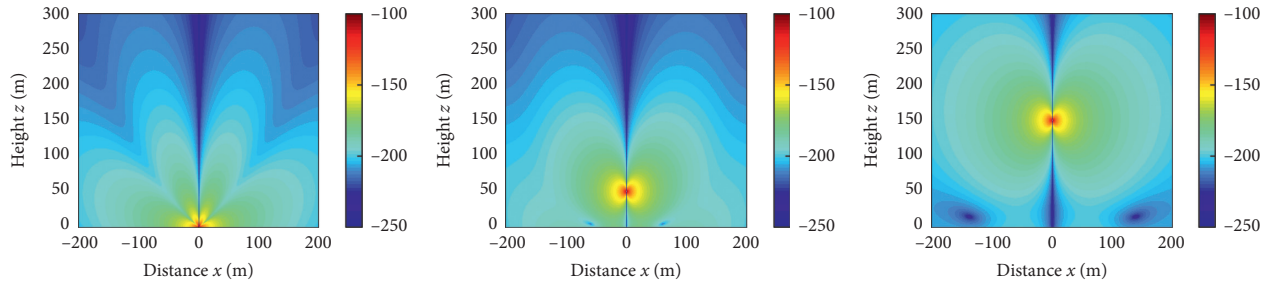

FIGURE 10: Field distribution of $E_{2\varphi}$ in the x-z plane: (a) $d = 0$ m, (b) $d = 50$ m, and (c) $d = 150$ m.

Figures 9(c) and 10(c) is very likely to that in free space, which implies that when the height of the dipole is high enough away from the interface, the radiation result is nearly not affected by the sea water.

4. Conclusions

This paper deals with the integrals for the electromagnetic field of a vertical magnetic dipole lying above the boundary of a lossy half-space in order to derive analytical formulas for the near-zone field. On the basis of the feature of "quasi-static" state and the equivalent infinitesimal theory, we can induce two rational assumptions. One is $\gamma_2 \approx i\lambda$, and the other is about the substitution of $\gamma_1 - \gamma_2$. Comparisons with numerical solutions show that both the amplitude and phase are quite consistent with each other. Curves for contrast with the exact formulas are also drawn when the dipole source and observing point are both on the boundary, which is a further proof of the high accuracy and reliability of our manner. Simulations also show that different components have different validity limits of $k_2\rho$ for maintaining a consistency between the proposal and numerical solutions. The

smallest validity limit always occurs for the component H_{2z}, and the value of $k_2\rho$ should be no greater than 0.6 in order to keep a good consistency. Subsequent computations, which indicate that operating frequencies and the positions of the dipole source and the receiving point will all affect the field components, are also performed. In addition, it should be pointed out that these formulas are also suitable for other cases where the condition $k_1 \ll k_2$ is satisfied. And the media in two regions are interchangeable. Under this circumstance, $\gamma_1 \approx i\lambda$ is acquired, and the approximation in (13) changes to $|\gamma_2 - \gamma_1 - k_2|$. Then, by a similar method presented in this paper, the final field expression can be obtained.

Data Availability

All data are available as MATLAB code.

Conflicts of Interest

The authors declare that there are no conflicts of interest regarding the publication of this paper.

Acknowledgments

This work was supported in part by the National Science Foundation of China under Grant 61571389.

References

[1] US Navy, *Extremely Low Frequency Transmitter Site: Clam Lake, Wisconsin*, US Navy Fact File, Philadelphia, PA, USA, 2001.

[2] T. Jacobsen, *ZEVS, the Russian 82 Hz ELF Transmitter, an Extreme Low Frequency Transmission-System, Using the Real Long Waves*, ALFLAB, Halden, Norway, 2013, http://www.vlf.it/zevs/zevs.htm.

[3] "Technology in focus: underwater electromagnetic propagation," 2008, https://www.hydro-international.com/content/article/underwater-electromagnetic-propagation.

[4] G. Benelli and A. Pozzebon, *RFID under Water: Technical Issues and Applications RFID under Water: Technical Issues and Applications*, InTech, Rijeka, Croatia, 2013.

[5] A. Sommerfeld, "Über die Ausbreitung der Wellen in der drahtlosen Telegraphie," *Annalen der Physik*, vol. 333, no. 4, pp. 665–736, 1909.

[6] K. A. Norton, "The propagation of radio waves over the surface of the earth and in the upper atmosphere," *Proceedings of the Institute of Radio Engineers*, vol. 24, no. 10, pp. 1367–1387, 1926.

[7] W. L. Anderson, "Numerical integration of related hankel transforms of orders 0 and 1 by adaptive digital filtering," *Geophysics*, vol. 44, no. 7, pp. 1287–1305, 1979.

[8] I. Arun and M. Venkatapathi, "Analysis of numerical solutions to sommerfeld integral relation of the half-space radiator problem," *Applied Numerical Mathematics*, vol. 106, pp. 79–97, 2016.

[9] W. C. Chew, "A quick way to approximate a Sommerfeld-Weyl-type integral (antenna far-field radiation)," *IEEE Transactions on Antennas and Propagation*, vol. 36, no. 11, pp. 1654–1657, 1988.

[10] Y. Long, H. Jiang, and B. Rembold, "Far-region electromagnetic radiation with a vertical magnetic dipole in sea," *IEEE Transactions on Antennas and Propagation*, vol. 49, no. 6, pp. 992–996, 2001.

[11] D. Margetis and T. T. Wu, "Exactly calculable field components of electric dipoles in planar boundary," *Journal of Mathematical Physics*, vol. 42, no. 2, pp. 713–745, 2001.

[12] O. M. Abo-Seida, S. T. Bishay, and K. M. El-Morabie, "Far-field radiated from a vertical magnetic dipole in the sea with a rough upper surface," *IEEE Transactions on Geoscience and Remote Sensing*, vol. 44, no. 8, pp. 2135–2142, 2006.

[13] H. Wang, K. Yang, and K. Zheng, "Electromagnetic field radiated in air from a horizontal/vertical magnetic dipole in sea," *Journal of Electromagnetic Waves and Applications*, vol. 29, no. 7, pp. 858–873, 2015.

[14] S. T. Bishay, O. M. Abo-Seida, and H. S. Shoeib, "Analytical formulas for dipole radiation buried inside planar stratified media," in *Proceedings of the International Conference on Aerospace Sciences and Aviation Technology (ASAT-16)*, Cairo, Egypt, May 2015.

[15] R. W. P. King, M. Owens, and T. T. Wu, *Lateral Electromagnetic Waves: Theory and Applications to Communications, Geophysical Exploration, and Remote Sensing*, Springer-Verlag, New York, NY, USA, 1992.

[16] H. L. Xu, T. T. Gu, and K. Li, "Approximated solutions for ELF near-field propagation due to a horizontal electric dipole excitation near the sea-rock boundary," *IEEE Transactions on Antennas and Propagation*, vol. 66, no. 5, pp. 2471–2481, 2018.

[17] A. J. Banos and J. P. Wesley, "The Horizontal Dipole in a Conducting Half-Space," University of California," Marine Physical Laboratory, San Diego, CA, USA, 1953.

[18] S. Durrani, "Air-to-undersea communication with electric dipoles," *IRE Transactions on Antennas and Propagation*, vol. 10, no. 5, pp. 524–528, 1962.

[19] S. Durrani, "Air to undersea communication with magnetic dipoles," *IEEE Transactions on Antennas and Propagation*, vol. 12, no. 4, pp. 464–470, 1964.

[20] P. R. Bannister, "Quasi-static fields of dipole antennas at the earth's surface," *Radio Science*, vol. 1, no. 11, pp. 1321–1332, 1966.

[21] P. R. Bannister, *New Formulas that Extend Norton's Farfield Elementary Dipole Equations to the Quasi-Near Field Range*, Naval Underwater Systems Center, New London CT, USA, 1984.

[22] J. R. Wait, "The magnetic dipole over the horizontally stratified earth," *Canadian Journal of Physics*, vol. 29, no. 6, pp. 577–592, 1951.

[23] R. E. Collin, "Some observations about the near zone electric field of a hertzian dipole above a lossy earth," *IEEE Transactions on Antennas and Propagation*, vol. 52, no. 11, pp. 3133–3137, 2004.

[24] L. C. Zhang, Y. M. Wang, and T. Guo, "Research of extremely low frequency to magnetic dipole in seawater media," in *Proceedings of the International Conference on Information and Communications Technologies (ICT)*, Rennes, France, May 2015.

[25] M. Dautta, "Computation of electromagnetic field propagation characteristics of a dipole antenna submerged in seawater," in *Proceedings of the International Conference on Wireless Communications, Signal Processing and Networking (WiSPNET)*, Chennai, India, March 2016.

[26] A. S. Imm and A. C. Fraser-Smith, "Further investigation of the interference minimums in the low-frequency electromagnetic fields produced by a submerged vertical magnetic dipole," *Radio Science*, vol. 25, no. 4, pp. 339–347, 1990.

[27] M. Parise, "Exact electromagnetic field excited by a vertical magnetic dipole on the surface of a lossy half-space," *Progress In Electromagnetics Research B*, vol. 23, pp. 69–82, 2010.
[28] J. A. Kong, *Electromagnetic Wave Theory*, EMW Publishing, Cambridge, UK, 2008.
[29] R. W. P. King, "Electromagnetic field of a vertical dipole over an imperfectly conducting half-space," *Radio Science*, vol. 25, no. 2, pp. 149–160, 1990.